Organic & Biomolecular Chemistry

ROYAL SOCIETY OF CHEMISTRY

PAPER

View Article Online
View Journal | View Issue

Cite this: *Org. Biomol. Chem.*, 2024, **22**, 2252

2,4,5-Triaminopyrimidines as blue fluorescent probes for cell viability monitoring: synthesis, photophysical properties, and microscopy applications†

Jorge M. Gonçalves,[a,b] João N. D. Gonçalves,[a,c] Luís F. Sousa,[a,b] Lígia R. Rodrigues,[d,e] Paulo Correia-de-Sá,[f] Paulo J. G. Coutinho,[b] Elisabete M. S. Castanheira,[b] Rui Oliveira[c] and Alice M. Dias *[a]

Monitoring cell viability is critical in cell biology, pathology, and drug discovery. Most cell viability assays are cell-destructive, time-consuming, expensive, and/or hazardous. Herein, we present a series of newly synthesized 2,4,5-triaminopyrimidine derivatives able to discriminate between live and dead cells. To our knowledge, these compounds are the first fluorescent nucleobase analogues (FNAs) with cell viability monitoring potential. These new fluorescent molecules are synthesized using highly efficient and cost-effective methods and feature unprecedented photophysical properties (longer absorption and emission wavelengths, environment-sensitive emission, and unprecedented brightness within FNAs). Using a live–dead *Saccharomyces cerevisiae* cell and theoretical assays, the fluorescent 2,4,5-triaminopyrimidine derivatives were found to specifically accumulate inside dead cells by interacting with dsDNA grooves, thus paving the way for the emergence of novel and safe fluorescent cell viability markers emitting in the blue region. As the majority of commercially available viability dyes emit in the green to red region of the visible spectrum, these novel markers might be useful to meet the needs of blue markers for co-staining combinations.

Received 17th January 2024,
Accepted 14th February 2024

DOI: 10.1039/d4ob00092g

rsc.li/obc

1. Introduction

Small-molecule fluorescent probes have been extensively used for monitoring cell viability. Cell viability assays are critical for multiple studies in cell biology, pathology, and drug discovery, which span from antimicrobial research to disease pathophysiology and pharmacological drug development. Live–dead assays often use time-consuming cell-unrecoverable colorimetric reagents (*e.g.* MTT, XTT, and WST). In this regard, fluorescence imaging techniques are advantageous compared to the colorimetric ones, since they offer fast, highly sensitive and non-destructive alternatives, also allowing real-time *in situ* observations.[1] Countless fluorescent probes for cell viability (FPCV) assays have been developed; these are designed to detect changes in specific intracellular components and/or the physicochemical properties associated with cell death.[2] Despite these advantages, FPCVs exhibit complex molecular structures, which are often difficult to synthesize and may cause significant photodamage to the cell.[3] FPCVs are also unable to distinguish different cell stages.[4] Hence, the development of highly sensitive red-shifted biocompatible FPCVs acting through different mechanisms is of utmost importance in several research settings, for instance, to deepen our understanding of the pathophysiological mechanisms of cell death and to develop and screen new drugs.

Fluorescent nucleoside analogues (FNAs) have multiple applications in biochemical research,[5,6] which include their emerging roles as microenvironmental-specific bioimaging probes. Major hurdles concern the synthesis efficiency of fluorescent nucleobases, mostly due to the presence of multiple reactive functional groups.[7,8] The synthetic design is even

[a]*CQ-UM — Centre of Chemistry of University of Minho, Department of Chemistry, University of Minho, Campus de Gualtar, 4710-057 Braga, Portugal. E-mail: ad@quimica.uminho.pt*
[b]*CF-UM-UP — Physics Centre of Minho and Porto Universities and LaPMET (Laboratory of Physics for Materials and Emergent Technologies), Campus de Gualtar, 4710-057 Braga, Portugal*
[c]*CBMA — Centre of Molecular and Environmental Biology, Department of Biology, University of Minho, Campus de Gualtar, 4710-057 Braga, Portugal*
[d]*CEB — Centre of Biological Engineering, Department of Biological Engineering, University of Minho, Campus de Gualtar, 4710-057 Braga, Portugal*
[e]*LABBELS – Associate Laboratory, Guimarães, Braga, Portugal*
[f]*Laboratório de Farmacologia e Neurobiologia, Center for Drug Discovery and Innovative Medicines (MedInUP), Instituto de Ciências Biomédicas de Abel Salazar, Universidade do Porto, R. Jorge Viterbo Ferreira, 228, 4050-313 Porto, Portugal*
† Electronic supplementary information (ESI) available. See DOI: https://doi.org/10.1039/d4ob00092g

more challenging when optimal photophysical properties and/or intramolecular charge transfer characteristics towards microenvironment sensitivity are needed for live-cell imaging.[9–11] Chemical modifications to generate FNAs normally involve decorating commercial pyrimidines and purines with bulky and highly conjugated groups at C-2 or C-8, respectively, through cross-coupling condensation reactions.[12] The main constraints of FNAs for efficient and environmentally safe syntheses include the use of costly precursors and hazardous metal catalysts. The undesirable group-size effects have also limited nucleobase pairing and target recognition. Most FNAs developed so far exhibit near-UV emission and/or smaller Stokes shifts, which limit their use in live-cell fluorescence microscopy.[6,9] To the best of our knowledge, FNAs are rarely considered for live-cell viability assays, mostly due to their inadequate photophysical properties.

Due to the wide distribution of pyrimidines in natural products and functional materials, and their remarkable biological and pharmacological significance, a variety of methods for the synthesis of these molecules have been reported over the past few decades.[13] To obtain 2- or 4-amino, and 2,4- or 4,6-diaminopyrimidines, which are privileged structures in drug development, preferred methods involved the amination of the corresponding 2,4(4,6)-dihalopyrimidines by direct substitution with primary and secondary amines *via* SNAr reactions.[14,15] Nevertheless, the preparation of these halopyrimidine precursors from simple building blocks often involves the use of hazardous reagents/catalysts and harsh reaction conditions, also requiring multistep procedures. On the other hand, 4,5-diaminopyrimidines are the most versatile precursors for the synthesis of biologically relevant purines, pteridines and other bicyclic heterocycles. Yet, the synthesis of these less common diaminopyrimidines requires an additional incorporation of the 5-amino group, usually involving nitrosation or nitration at the 5-position by SEA followed by reduction reactions.[16] An alternative approach, which is one of the oldest methods to obtain 4,5-diaminopyrimidines, is the opening of the ring of purine precursors at the C-8 position.[17] Yet, this method generally demands the use of strong electrophiles to activate the N^7-position for ring-opening and a basic medium to facilitate the cleavage of the formyl group. Ring-opening in the acidic medium had only been achieved for N^7-substituted adenine derivatives, yielding the corresponding N^5-substituted 4,5,6-triaminopyrimidines. Reports on the acid hydrolysis of N^9-substituted purines to afford N^5-substituted 4,5-diaminopyrimidines were not found, and attempts to obtain 2,4,5-triaminopyrimidines by the hydrolysis of 2-aminopurines at C-8 have been particularly difficult to achieve.[18]

Using efficient and cost-effective strategies, new N^4-aryl 2,4,5-triaminopyrimidines with a cyano group at the C-6 position (**4**) were synthesized by our group from N^4-aryl 2-amino-6-cyanopurines **2**. These small-sized nucleobases exhibit excellent fluorescence properties with the highest quantum yields reported to date for this group of compounds, which are accompanied by outstanding Stokes shifts and environmental sensitivity. Preliminary microscopy tests and dsDNA interaction studies suggest that these molecules accumulate inside and specifically stain dead yeast cells, underpinning their putative use as a new class of cell viability markers emitting in the blue region of the visible spectrum. Strikingly, the majority of commercially available viability dyes emit in the green to red region of the visible spectrum, such as propidium iodide and SYBR Green I. Moreover, most fluorescent reporter constructs also encode for green to red fluorescent proteins such as GFP, YFP, and mCherry. This can be limiting to multiplex imaging due to the lack of combinations of contrasting colours which facilitate image analyses.[19,20] In addition, good colour separation is essential for detecting multiple entities using different fluorophores, which is achieved by ensuring minimal spectral overlap. Since most commercially available fluorophores emit in the green to red region, blue-emitting dyes provide means for tackling spectral overlap issues in multispectral techniques, as emission spectral overlap is minimized, particularly with red-emitting fluorophores, such as in fluorescence microscopy and flow cytometry.[21,22] Thus, the unique spectral properties of 2,4,5-triaminopyrimidines herein presented make them easily combinable with the most common green to red fluorescent markers. This enables new palettes of contrasting colour combinations which may be extremely useful for multicolour fluorescence imaging.

2. Results and discussion

2.1. Synthesis of 2,4,5-triaminopyrimidines

Previously, highly fluorescent 2-amino-6-cyanopurines **2** were synthesized through condensation reactions of imidazole precursors with cyanamide, followed by cyclization of key intermediates **1** (Scheme 1).[23] Aiming to generate new fluorescent analogues, the reactivity of this new purine scaffold was investigated. Attempts to modify the 6-cyano group revealed that purines **2** with 9-aryl substituents undergo ring-opening of the imidazole moiety upon heating in acidic media, which generates new N^4-substituted 2,4,5-triaminopyrimidines **3**. To find the reaction conditions that favour ring-opening, preliminary tests involving the heating of cyanopurines **2** in ethanol and 12 M hydrochloric acid at 80 °C were conducted. After 1–5 days, mixtures of the desired product and the starting purines **2** were isolated, and no appreciable changes in the composition of the isolated mixtures, or in the reaction times, were detected when different amounts of acid (2.5–8.0 equivalents) were

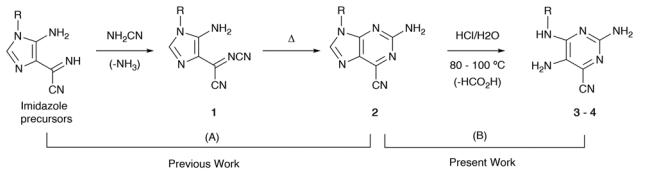

Scheme 1 (A) Previously developed pathway for the synthesis of 2-amino-6-cyanopurines **2** from imidazole precursors; (B) synthesis of the new 2,4,5-triaminopyrimidines **3–4** presented here.

used. In contrast, increasing the reaction temperature up to 100 °C not only favoured the reaction rate, but also solved the problems of the limited solubility of the starting reagent **2**. As it was observed that the lower the purine **2** solubility, the longer the time required for the completion of the reaction, certain starting reagents **2** required higher temperatures for reaction completion and/or the addition of a co-solvent with a higher boiling point (DMSO). Finally, the use of different amounts of acid under these conditions revealed that 2.5 equivalents was the optimum amount, regardless of the substituent. Based on these results, the hydrolysis of a series of 9-aryl 2-amino-6-cyanopurines **2** was achieved by stirring the starting reagents with 2.5 equivalents of 12 M hydrochloric acid in ethanol (or a mixture of ethanol/DMSO) at 80 or 100 °C for 1 day (Scheme 2). The products, isolated in 50-85% yields as green solids, were characterized by NMR spectroscopy and the obtained data enable their identification with the structures of HCl salts **3**. Finally, thin layer chromatography (TLC) analysis revealed that these compounds exhibit intense blue-cyan fluorescence under UV light. After optimizing the conditions for the synthesis of salts **3**, a neutralizing step of the isolated solids was also performed to characterize the neutral form and investigate the effect of protonation on the photophysical properties of this new group of compounds. For this purpose, compounds **3** were neutralized with triethylamine (2.5 equivalents) in acetonitrile, and their neutral forms were successfully isolated with 78–97% yields. TLC analysis of these solids also showed an intense blue fluorescent spot under UV light.

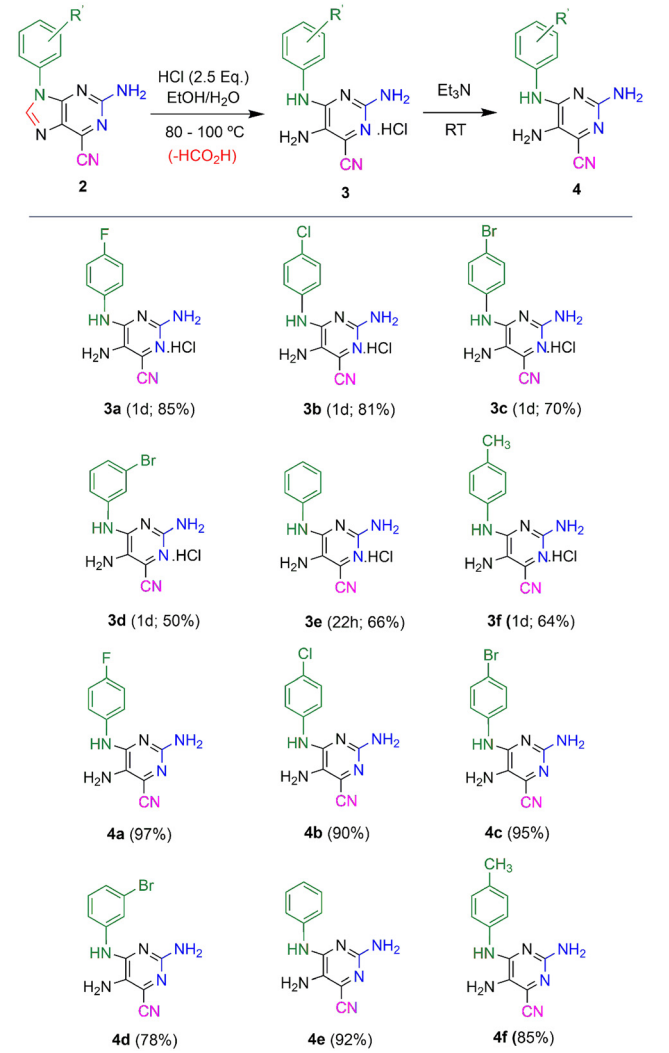

Scheme 2 Compound **2** was combined with 37% hydrochloric acid (2.5 equivalents) at 80 or 100 °C in ethanol (or a mixture of ethanol/DMSO). Then, pyrimidines **3** were isolated by filtration. After that, they were neutralized with triethylamine in acetonitrile and subsequently isolated by filtration affording pyrimidines **4**.

According to the proposed mechanism presented in Scheme 3, these reactions should start when hydrochloric acid protonates the N-7 nitrogen of the purine ring, as the C-8 carbon becomes susceptible to nucleophilic attack. The water present in the reaction mixture might attack the purine ring at this position, leading to the formation of a tetrahedral intermediate that undergoes the opening of the five-membered ring, thus generating a pyrimidine-based formamide intermediate. This formamide group is also sensitive to cleavage in an acidic medium by hydrolysis and elimination of one molecule of formic acid, leading to compounds **3**.

Full characterization of the new compounds by NMR (^{1}H, ^{13}C NMR, HSQC and HMBC techniques) and IR spectroscopy, and mass spectrometry are presented in Fig. S13–S36 (ESI†). The ^{1}H NMR spectra of compound **3** indicate that the highest chemical shift signal was assigned to the NH group, which appears as a broad singlet at δ 9.9–10.8 ppm. Signals from the protons of the phenyl group appear as doublets or triplets, depending on the number of their neighbouring protons. Their chemical shifts vary in the region δ 6.9–7.9 ppm, according to the effect of the substituent group present on the benzene ring. In these spectra, it was not possible to observe the NH_2 signals because the molecules were in their protonated form. Concerning compounds **4**, it was observed that chemical shifts tend to lower values. For instance, the NH signal was observed at δ 9.7–10.7 ppm in the protonated form **3**, which shifted towards δ 8.6–9.7 ppm in the neutral form, evidencing the absence of the positive charge in the molecule.

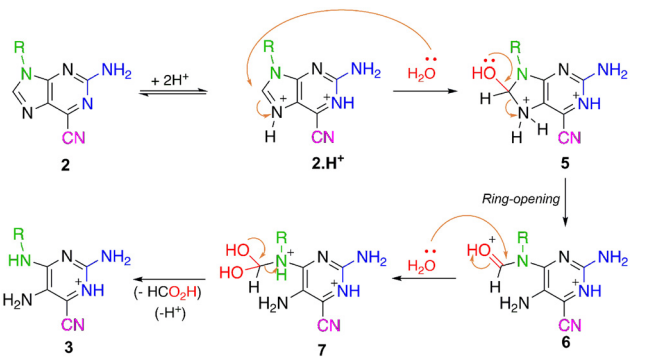

Scheme 3 Proposed mechanism for the synthesis of 2,5-diaminopyrimidines **3** from 6-cyano-2-aminopurines **2**.

In the ^{13}C NMR spectra of compounds **3**, the signals assigned to the pyrimidine carbons linked to the amino groups were recorded at δ 150 ppm (C-2), δ 130 ppm (C-5) and δ 153 ppm (C-6). A typical signal of the 6-nitrile group was observed at δ 112–113 ppm, thus confirming its presence in their structure. In compounds **4**, it was verified that the corresponding signals tend to show higher chemical shift values when compared to compounds **3**.

2.2. Photophysical characterization

The photophysical characterization of compounds **3** and **4** comprised the determination of the maximum absorption and emission wavelengths, Stokes shifts, fluorescence quantum yields and molar absorption coefficients (Tables S1–S4 and Fig. S37–S40, ESI†). Molar absorption coefficient values are very reasonable, in the range of 1–2.5 × 10^4 M^{-1} cm^{-1} (or slightly below) and point to allowed transitions from the ground to the excited electronic state. Overall, both groups of compounds present low fluorescence quantum yields in protic solvents, due to solute–solvent hydrogen bonding. However, the yields are significantly higher in non-protic solvents. By comparing the neutral and protonated forms of these compounds, one can conclude that the emission quantum yield increases in the neutral form when non-protic solvents (*e.g.* dioxane and dichloromethane) are used, while it decreases in protic solvents, such as aqueous buffer solutions, which is particularly useful in microenvironment-monitoring applications.[24] Considering absorption and emission wavelengths, some differences were detected when comparing compounds **3** and **4** (Fig. 1), from which the sensitivity differs with solvent polarity (Fig. S37–S40, ESI†).

Triaminopyrimidines reported here exhibit red-shifted absorption and emission maxima within FNAs due to their unique substituent patterns. The reported fluorescent pyrimidine analogues exhibit absorption in the region of 290–330 nm and emission in the region of 374–430 nm, whereas these newly prepared pyrimidines show absorption near 360 nm, emission near 470 nm, and large Stokes shifts (*S* = 83 nm in aqueous buffer and 108 nm in dioxane). In addition, they also exhibit very high fluorescence quantum yields (Φ_F = 0.5–0.6 in dioxane) and brightness (some $\varepsilon{\cdot}\Phi_F$ values around 15 000 M^{-1} cm^{-1}) when compared with the two brightest reported pyrimidine analogues which presented brightness of $\varepsilon{\cdot}\Phi_F$ = 2000 M^{-1} cm^{-1} and 3800 M^{-1} cm^{-1}.[6,25]

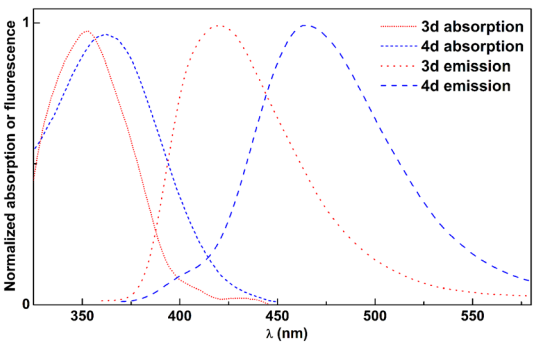

Fig. 1 Normalized absorption and fluorescence spectra of 2.5 × 10^{-6} M solutions of compounds **3d** and **4d** in dioxane, as an example.

2.3. Live–dead fluorescence cell assay and cytotoxicity test

To assess the putative role of the novel 2,4,5-triaminopyrimidines as fluorescent cell viability probes, we used a live–dead yeast cell assay. To this end, cultures of the yeast *Saccharomyces cerevisiae* were co-stained with 2,4,5-triaminopyrimidines (blue channel) and propidium iodide (PI, red channel), used as a reference cell death marker. The results show that most living cells exclude signals detected in the blue fluorescence channel when the cells were incubated with compound **3d** (Fig. 2). The same occurred for other 2,4,5-triaminopyrimidines (Fig. S43, ESI†). Few living cells, however, incorporate the red fluorescent probe corresponding to PI. The influx of PI through the membranes of living cells has been reported before.[26,27] The fluorescence intensities of compounds **3b–3e** dramatically increased in PI-positive dead yeast

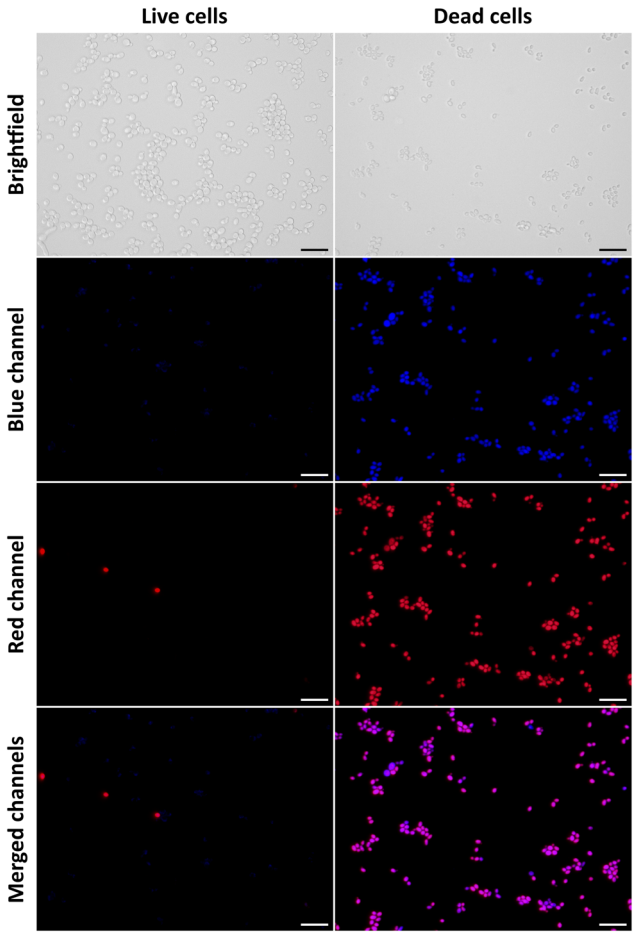

Fig. 2 Live and dead *Saccharomyces cerevisiae* BY4741 cells double stained with propidium iodide and compound **3d** (10 μM and 250 μM, respectively; 15 min incubation at room temperature in PBS pH 7.2, protected from light). The death of cells was achieved by heat treating the cells at 80 °C for 2 min in a water bath. Scale bar = 20 μm.

cells (Fig. 2 and Fig. S43, ESI†). Moreover, small dots were also found in dead cells treated with compounds **3b** and **3e** (Fig. S43, ESI†), and their nature is yet to be determined. Surprisingly, no significant increase in fluorescence was observed in live or dead yeast cells incubated with compounds **3a** and **3f** (not shown). Overall, data indicate that several novel 2,4,5-triaminopyrimidines can fluorescently label dead yeast cells, possibly with fewer false positives than the widely used cell-death indicator, PI.

For the sake of cell viability assay validation, the new 2,4,5-triaminopyrimidines were also tested for cytotoxicity. The growth rates of *S. cerevisiae* cultures in the absence and the presence of 2,4,5-triaminopyrimidines were determined and the results show that most 2,4,5-triaminopyrimidines failed to affect yeast cell proliferation compared to control conditions without drug addition (Fig. 3, no statistically significant changes were detected, P value >0.05). The only exception was compound **3c**, which extended the lag phase of the culture, indicating a toxic effect (Fig. 4).

2.4. dsDNA interaction studies

The fluorescence microscopy results prompted us to perform a dsDNA interaction assay with compound **4d** through fluorescence (Fig. 5; see experimental details in the ESI†). The observed fluorescence intensity increases with higher DNA concentrations, reaching a limit value for [DNA]/[**4d**] ratios ≥30, indicating that total compound binding was achieved at this [DNA]/[**4d**] ratio. The binding constant and binding site size were determined using the modified Scatchard equation, given by McGhee and von Hippel[28] (see the ESI†).

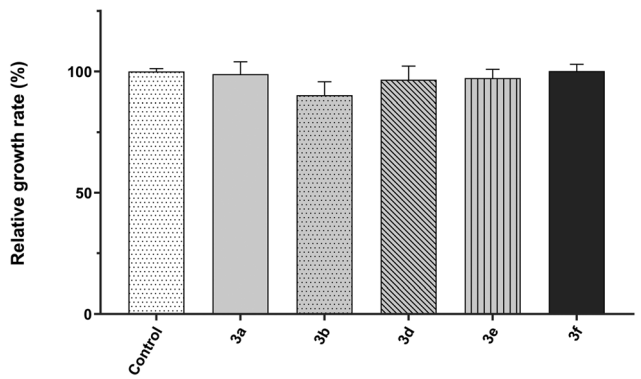

Fig. 3 Relative growth rates of the *Saccharomyces cerevisiae* strain BY4741 incubated at 30 °C with 200 rpm in SD medium in the presence of 1% DMSO (control, solvent of the compounds) or 2,4,5-triaminopyrimidines **3** (**3a**, **3b**, **3c**, **3d**, **3e** or **3f**). Growth was monitored by measuring the optical density at 600 nm, growth rates were calculated, and the mean relative growth percentages were determined taking the control as the reference. Data are presented as mean ± standard deviation from three independent replicas. Statistical analysis was performed through one-way ANOVA followed by Dunnett's multiple comparison test to compare with the control conditions and no statistically significant changes were detected (P value >0.05). The growth rate in the presence of compound **3c** was not calculated due to a very prolonged lag phase (see Fig. 4).

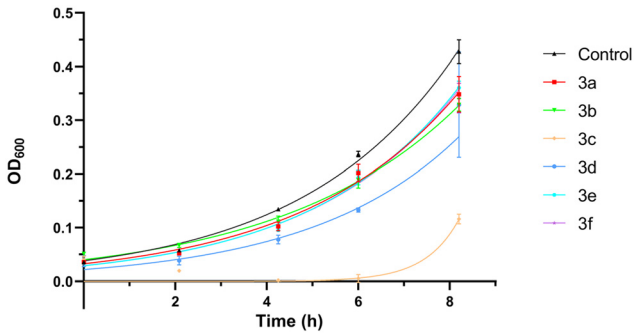

Fig. 4 Growth curves of the *Saccharomyces cerevisiae* strain BY4741 in the presence of compounds **3** (**3a**, **3b**, **3c**, **3d**, **3e** or **3f**) or 1% DMSO (control, solvent of the compounds). The microcultures were prepared in SD medium in 96-well plates and incubated at 30 °C and 200 rpm and growth was monitored by measuring the optical density at 600 nm. Data are presented as mean ± standard deviation from three independent replicas.

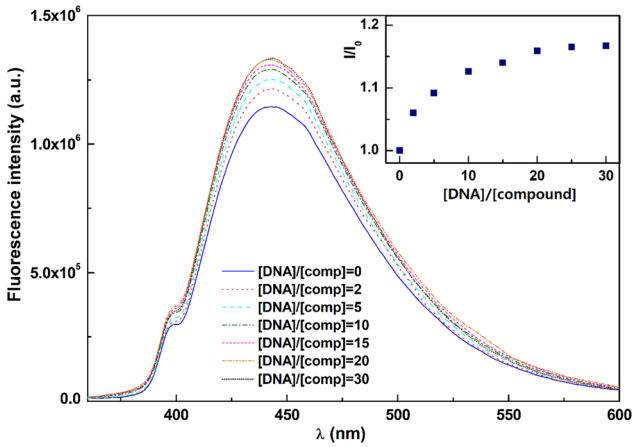

Fig. 5 Emission spectra of compound **4d** with increasing DNA concentration. Inset: Ratio of the maximum emission intensities in the absence (I_0) and the presence (I) of DNA at several [DNA]/[**4d**] ratios.

The fluorescence measurement results were fitted by least squares methods, allowing us to obtain a reasonably high binding constant of $K_i = (4.1 \pm 0.5) \times 10^5\ M^{-1}$ and $n = 5 \pm 0.6$. These results are similar to the ones previously obtained for other polycyclic aromatic molecules.[29]

To further investigate the interaction between compound **4d** and dsDNA, *i.e.*, through intercalation or groove binding, fluorescence quenching experiments with iodide ions were also performed for the solution with [DNA]/[**4d**] = 30 (Fig. 6). The quenching data were first plotted according to the Stern–Volmer relation (Fig. 6A).[30] The Stern–Volmer plot is non-linear, exhibiting a downward curvature, which means that not all fluorescent molecules are accessible to the quencher. In this case, some compounds are accessible to the quencher and other molecules are not accessible and therefore the Stern–Volmer equation must be modified as described by others.[31] The modified equation (see the ESI†) allows the determination

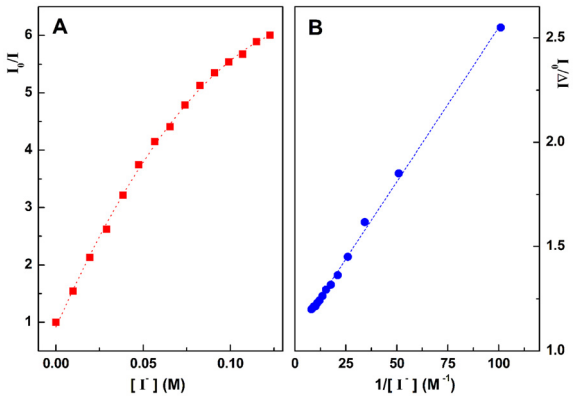

Fig. 6 (A) Stern–Volmer plot for quenching with iodide ions. (B) The corresponding modified Stern–Volmer plot.

of a 93% fraction of accessible molecules (f_a = 0.93) (Fig. 6B). This would correspond to the percentage of non-intercalated molecules, with the major fraction of **4d** possibly binding to DNA grooves.

The observed increase in fluorescence (Fig. 5) and the fluorescence microscopy results (Fig. 2) led us to conclude that the 2,4,5-triaminopyrimidines and PI may share the same staining mechanism through dsDNA binding after penetrating dead cells lacking the plasma membrane barrier. These results do not exclude the possibility that both DNA fluorescent dyes may enter living cells *via* regulated plasma membrane transport, but even after discounting this bias, the net influx into living cells should be considerably much lower compared to dead and/or dying cells. Taking this into account, the mechanisms underlying the putative transport of the new 2,4,5-triaminopyrimidines across the plasma membrane and their stability/compartmentalization inside living cells also remain to be determined, which might affect fluorescence signals.

2.5. Molecular docking

Further information on the binding preferences of the studied compounds with dsDNA can be obtained through molecular docking simulations using *Autodock4*,[32] as used in other published works.[33,34] The crystallographic structures of a native dsDNA dodecamer (PDB ID 1hq7), proflavine (profl.) intercalated in a dsDNA hexamer (PDB ID 3 ft6) and a diamidine derivative (X8 V) groove-bound to a dsDNA dodecamer (PDB ID 7kwk) were used in docking studies by keeping only the polynucleotide structure.

Table 1 shows the obtained results for compounds in the protonated form **3a–f** and in the neutral form **4a–f**, and for the ligands that were removed from the starting crystallographic structures. The latter cases allow the validation of the docking procedure effectiveness and provide reference values for comparison with the studied compounds. Additionally, propidium iodide (PI), a well-known DNA intercalator, was also docked into 3 ft6.

Fig. S44 (in the ESI†) shows examples of the obtained docking poses. It can be concluded that the compounds intercalate into DNA with binding energies similar to those of proflavine, especially in the case of the protonated forms. Binding energies are more favourable for groove binding, although the reference compound thiophene diamidine is much more effective. The obtained results confirm the experimental evidence obtained from the fluorescence quenching experiments in the previous section. In the same way, reports on the lower dielectric constant of DNA grooves[35,36] seems to be in line with the increased emission quantum yield observed for the neutral form in non-protic solvents, supporting the enhanced fluorescence observed in the bioimaging of dead cell assays.

2.6. *Ab initio* molecular quantum chemistry calculations

The electronic and structural properties of compound **4d** were studied by *ab initio* molecular quantum chemistry calculations using Gaussian 09 software[37] with a 6-31++G** basis set using the TD-SCF DFT method with the MPW1PW91 functional and a continuous solvation model (PCM-polarizable continuum model) corresponding to ethanol. Ground state and first excited state equilibrium geometries for the neutral form are shown in Fig. S45 (ESI†). The molecule is planar in the ground state with the phenyl ring going 32° out-of-plane upon electronic excitation. The corresponding S_0–S_1 transitions are 362.7 nm and 474.6 nm with oscillator strengths of 0.544 and 0.396, respectively. Using FCclasses3,[38] it is possible to calculate absorption/emission spectra. The results showed a very low molar absorptivity coefficient, explained by the large geometry variation upon electronic excitation. As experimental

Table 1 Binding energies (kcal mol^{-1}) of various compounds (Cpd.) in dsDNA sequences (3ft6, 7kwk, 1hq7)

dsDNA	3ft6		7kwk		1hq7	
Cpd.	**3** (protonated)	**4** (neutral)	**3** (protonated)	**4** (neutral)	**3** (protonated)	**4** (neutral)
3a/4a	−8.20	−7.54	−8.54	−8.48	−9.36	−9.62
3b/4b	−8.32	−7.87	−9.13	−9.43	−9.80	−9.90
3c/4c	−8.19	−7.95	−9.51	−9.75	−9.90	−9.51
3d/4d	−8.80	−8.46	−9.61	−9.46	−10.36	−10.74
3e/4e	−8.17	−7.68	−8.49	−8.67	−9.36	−9.65
3f/4f	−8.23	−7.68	−8.76	−8.98	−9.32	−9.92
profl.	−8.83	−8.61				
X8V			−12.73			
PI	−10.32					

values are orders of magnitude higher, we hypothesized that additional molecules, such as solvent and ions, could be stabilizing the planarity of the excited state. So, an explicit water molecule was added in the vicinity of both the amino group acting as the bridge and the amino group in the pyrimidine ring. Indeed, hydrogen bonds between the water molecule and the amino groups are formed and the change in planarity corresponds to 21°. Chlorine atoms are expected to be present, so we thought of using fluoride, as it has a lower impact on computational resources of the quantum mechanical calculations. A planar geometry of the excited state was obtained and the electron density variations upon S_0–S_1 excitation are shown in Fig. 7, for both neutral and protonated forms in ground and first excited state equilibrium geometries. For the neutral form, the S_0–S_1 transitions occur at 400.8 nm and 490.2 nm with oscillator strengths of 0.581 and 0.491, respectively, while for the protonated form, the S_0–S_1 transitions occur at 387.0 nm and 473.0 nm with oscillator strengths of 0.702 and 0.588, respectively.

It can be observed that the π-electron system spans all across the molecule including the two primary amines and through the secondary amine connecting the pyrimidine to the substituted phenyl, thus extending conjugation. Upon electronic excitation to the first excited state, the main changes in the electron distribution are a decrease in π-electron density in the amines, an increase in the cyano group and an increase in the phenyl moiety.

After all equilibrium geometry calculations, a frequency analysis was performed to make sure the program didn't stop at a saddle point (local maximum on the potential energy surface corresponding to a transition state), which would result in the appearance of imaginary frequencies.

Taking the obtained vibrational normal modes, it is possible, using, for example, FCclasses3, to make a vibronic analysis that can predict the form of the absorption and emission spectra. The results are shown in Fig. 8, together with the experimental spectra for the neutral form.

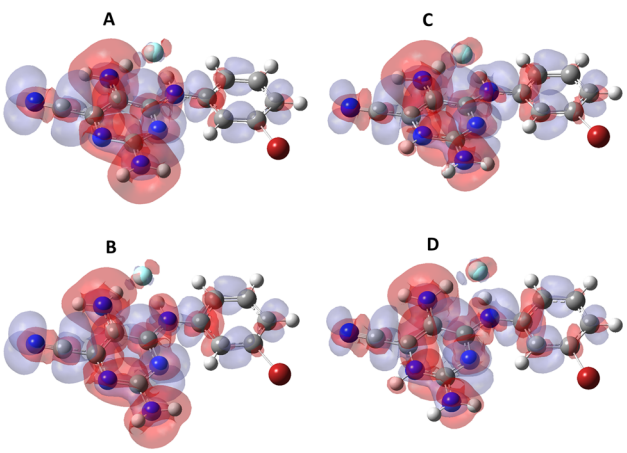

Fig. 7 Increase (blue) and decrease (red) of electron density upon electronic excitation of the neutral (A and B) and protonated (C and D) forms of compound **4d** in the ground state (B and D) and the first excited state (A and C) equilibrium geometry, using the MPW1PW91 functional. Carbon atoms: grey; hydrogen atoms: white; nitrogen atoms: blue; bromine atom: red; fluorine atom: cyan.

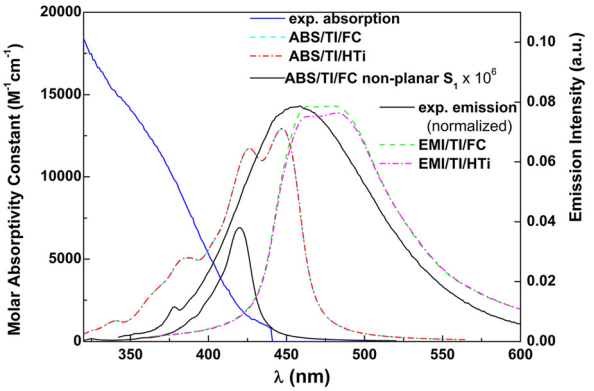

Fig. 8 Experimental *vs.* calculated absorption (one photon absorption, OPA) and emission (EMI) spectra using the MPW1PW91 functional for compound **4d** in ethanol.

FCclasses3 calculations are based on the harmonic approximation of the potential energy surfaces (PESs). We chose to use a constant transition dipole moment (Franck–Condon, FC) or allow its linear variation with the nuclear coordinates of the initial state (Herzberg–Teller, HT_i, non-Condon effect). We used the Adiabatic Hessian method as it takes into account both ground and excited state equilibrium geometries. This method was shown to give equivalent results to the more intuitive Vertical Hessian (VH) method.[39] The calculated spectra were obtained at 25 °C using a Lorentzian broadening with 0.4 eV HWHM and selection of hot states through a Boltzmann threshold of 0.1 (initial state i is selected if $\exp(-E_i/k_BT) > 0.1$).

A reasonable accordance was observed between the experimental emission spectral shape and the simulated spectral shape. A red-shift of ~20 nm is related to the usual underestimation of excitation energies in TD-SCF DFT methods. The shape of the simulated absorption spectrum is much different from the experimental one, which indicates that electronic excitations to higher excited states (S_0–S_n, $n > 1$), not accounted for in the simulated spectrum, have a dominating contribution. The energy difference between the equilibrium geometries of both states is 443 nm. The transitions that occur in the red tail correspond to hot states, whose importance stems from the presence of various low frequency modes (Table S5 in the ESI†). Nevertheless, the experimental molar absorptivity of compound **4d** in ethanol at the first shoulder (~435 nm) is 1.0 × 10^3 M^{-1} cm^{-1}, which is not too far from the one obtained in the simulated spectrum at the maximum absorption wavelength.

3. Conclusions

A series of novel N^4-aryl 2,4,5-triamino-6-cyanopyrimidines were obtained, both in hydrochloride salt (**3**) and neutral (**4**)

forms, by the acid ring-opening of previously prepared highly fluorescent 2-amino-6-cyanopurines **2**. These newly prepared 2,4,5-triaminopyrimidines exhibit longer absorption and emission spectral wavelengths and good brightness (between 5400 and 18 000 M^{-1} cm^{-1}) compared to other known FNAs. In addition, the newly synthesized compounds possess interesting environmental sensitivity, increasing the emission quantum yields in non-protic solvents. This demonstrates that the 2,4,5-triamino-6-cyanopyrimidine scaffold is an exceptional fluorophore, where the strong push–pull electronic structure resulting from the interplay between amino donors and nitrile acceptors may be responsible for their remarkable photophysical properties, as indicated by *ab initio* calculations. These characteristics may be valuable in cell biology, pathology, and drug development, given their ability to discriminate between live and dead cells, at least using the eukaryotic cell model organism *S. cerevisiae*. Their binding mechanism as DNA groove binders was disclosed by theoretical and experimental evidence. The lack of viability cell markers in the blue fluorescence spectrum highlights the importance of these 2,4,5-triaminopyrimidines as valuable alternatives to the most common green and red markers, paving the way for new fluorophore combinations and adding alternatives for spectral overlap issues.

Although the absorption wavelength is still in the UV region and the molar absorption coefficients are not so high, the chromophore scaffold reported here is promising for further development of new FNAs with improved photophysical properties and new applications.

4. Experimental

4.1. Materials and instruments

All compounds were fully characterized by elemental analysis and spectroscopic data. The NMR spectra, including the ^{1}H-^{13}C correlation spectra (HSQC and HMBC), were recorded at room temperature on a Bruker Avance 3400 (^{1}H: 400 MHz, ^{13}C: 100 MHz). The coupling constants, *J*, are reported in hertz (Hz). For the ^{1}H NMR analysis, about 3 mg of solid were used, while for the ^{13}C NMR analyses, about 20 mg were used. The solvent used in both cases was deuterated dimethylsulfoxide (DMSO-d_6). Infrared spectra were recorded using a FT-IR Spectrum Two – PerkinElmer. Melting points were determined on a Stuart cat. SMP3. The reactions were monitored by thin layer chromatography (TLC) using silica gel 60 F254 (Merck). The melting points were determined on a Stuart SMP3 melting point apparatus and are uncorrected.

UV-visible absorption spectra were recorded using a Shimadzu UV-3600 Plus spectrophotometer. Fluorescence emission spectra were recorded using a Fluorolog 3 spectrofluorimeter, with double monochromators in both excitation and emission. The emission spectra were corrected for the instrumental response, and absorbance at the excitation wavelength was kept below 0.1, to avoid the inner filter effect. Spectroscopic grade solvents (from Sigma-Aldrich/Merck) and Milli-Q grade water were used for the preparation of all solutions.

The fluorescence quantum yields were determined by the standard method[40] using eqn (1),

$$\Phi_s = \frac{A_r F_s {n_s}^2}{A_s F_r {n_r}^2} \Phi_r \quad (1)$$

where *A* is the absorbance at the excitation wavelength, *F* is the integrated emission area and *n* is the index of refraction of the solvents used. Subscripts refer to the reference (r) or the sample (s) compound.

Quinine sulphate in 0.05 M H_2SO_4 aqueous solution was used as the reference, $\Phi_r = 0.546$ at 25 °C.[41]

4.2. Synthesis

4.2.1. General procedure for the synthesis of 2-amino-6-cyanopurine derivatives 1. A green suspension of 5-aminoimidazole-4-carbimidoyl cyanide **1** (0.5–2.5 mmol) in acetonitrile (15 mL) was heated at 80 °C, under pressure, in the presence of trifluoroacetic acid (0.2 M equiv.), thus forming 2-aminopurine-6-carbonitriles **2**, until the starting material was totally consumed, as evidenced by TLC. After 1 hour–1 day, the green suspension was cooled in an ice-water bath for a few minutes. The solid formed was filtered and washed with ACN and diethyl ether leading to compounds **2**.

*4.2.1.1. 2-Amino-9-(4-fluorophenyl)-9H-purine-6-carbonitrile (**2a**).* Compound **1a** (0.61 g; 2.4 mmol), acetonitrile and trifluoroacetic acid. Compound **2a** was isolated, after 16 h, as a light yellow solid (0.49 g; 2.0 mmol; 82%). Mp >300 °C. ^{1}H NMR (400 MHz, DMSO-d_6): δ 7.19 (s, 2H), 7.44 (t, J = 8.8 Hz, 2H), 7.84 (dd, J = 9.2, 4.8 Hz; 2H), 8.67 (s, 1H) ppm; ^{13}C NMR (100 MHz, DMSO-d_6): δ 114.4, 116.4 (d, J = 23.0 Hz), 126.1 (d, J = 9.0 Hz), 128.5, 130.3, 130.4 (d, J = 2.0 Hz), 145.2, 154.8, 160.9, 161.3 (d, J = 244.0 Hz) ppm. IR (Nujol mull): ν 3493 m (NH), 3314 m (NH), 3204 m (NH), 2240 w (CN), 1643 s (C═N) cm^{-1}. Anal. Calcd for $C_{12}H_7FN_6$ (254.22): C, 56.69; H, 2.78; N, 33.06; found: C, 56.85; H, 2.87; N, 32.68.

*4.2.1.2. 2-Amino-9-(4-chlorophenyl)-9H-purine-6-carbonitrile (**2b**).* Compound **1b** (0.12 g; 0.44 mmol), mixture H_2O (1.0 mL)/DMSO (0.1 mL) and trifluoroacetic acid. Compound **2b** was isolated, after 2 h, as a brown solid (0.11 g; 0.41 mmol; 93%). Mp 229–230 °C. ^{1}H NMR (300 MHz, DMSO-d_6): δ 7.22 (s, 2H), 7.67 (d, J = 9.2 Hz, 2H), 7.88 (d, J = 8.8 Hz, 2H), 8.74 (s, 1H) ppm; ^{13}C NMR (75 MHz, DMSO-d_6): δ 114.4, 125.2, 128.6, 129.5, 130.3, 132.4, 133.0, 144.9, 154.7, 160.9 ppm. IR (Nujol mull): ν 3465 m (NH), 3313 m (NH), 3202 m (NH), 3107 w (NH), 2238 w (CN), 1643 s (C═N) cm^{-1}. Anal. Calcd For $C_{12}H_7ClN_6$ (270.68): C, 53.25; H, 2.61; N, 31.05; found: C, 54.09; H, 3.00; N, 31.17.

*4.2.1.3. 2-Amino-9-(4-bromophenyl)-9H-purine-6-carbonitrile (**2c**).* Compound **1c** (0.50 g; 1.59 mmol), acetonitrile and trifluoroacetic acid. Compound **2c** was isolated, after 19 h, as a light yellow solid (0.34 g; 1.08 mmol; 67%). Mp >298 °C. ^{1}H NMR (400 MHz, DMSO-d_6): δ 7.21 (s, 2H), 7.76 (d, J = 8.0 Hz, 2H), 7.80 (d, J = 8.0 Hz, 2H), 8.72 (s, 1H) ppm; ^{13}C NMR

(100 MHz, DMSO-d_6): δ 114.3, 120.7, 125.3, 128.6, 130.3, 132.3, 133.4, 144.7, 154.5, 160.8 ppm. Anal. Calcd For $C_{12}H_7BrN_6$ (315.13): C, 45.74; H, 2.24; N, 26.67; found: C, 45.66; H, 2.37; N, 26.53.

*4.2.1.4. 2-Amino-9-(3-bromophenyl)-9H-purine-6-carbonitrile (**2d**).* Compound **1d** (0.26 g; 0.90 mmol), acetonitrile and trifluoroacetic acid. Compound **2d** was isolated, after 4 h, as a light yellow solid (0.20 g; 0.64 mmol; 71%). Mp > 287 °C (Dec). ^{1}H NMR (400 MHz, DMSO-d_6): δ 7.25 (s, 2H), 7.54 (t, J = 8.4 Hz, 1H), 7.67 (ddd; J_1 = 8.0 Hz, J_2 = 2.0 Hz, J_3 = 1.2 Hz; 1H), 7.88 (ddd; J_1 = 8.0 Hz, J_2 = 2.0 Hz, J_3 = 1.2 Hz; 1H), 8.12 (t, J = 2.0 Hz, 1H), 8.77 (s, 1H) ppm; ^{13}C NMR (100 MHz, DMSO-d_6): δ 114.4, 122.0, 122.5, 126.1, 128.6, 130.3, 130.8, 131.4, 135.5, 144.9, 154.7, 160.9 ppm. IR (Nujol mull): ν 3455 m (NH), 3307 m (NH), 3198 m (NH), 3093 (=CH), 2177 w (CN), 1641 s (C=N) cm^{-1}. Anal. Calcd for $C_{12}H_7BrN_6$ (315.13): C, 45.74; H, 2.24; N, 26.67; found: C, 46.00; H, 2.56; N, 26.78.

*4.2.1.5. 2-Amino-9-phenyl-9H-purine-6-carbonitrile (**2e**).* Compound **1e** (0.41 g; 1.7 mmol), acetonitrile and trifluoroacetic acid. Compound **2e** was isolated, after 16 h, as a white solid (0.29 g; 1.2 mmol; 70%). Mp 259–271 °C. ^{1}H NMR (400 MHz, DMSO-d_6): δ 7.19 (s, 2H), 7.47 (t, J = 8.0 Hz, 1H), 7.59 (t, J = 8.0 Hz, 2H), 7.82 (dd, J_1 = 8.8 Hz, J_2 = 1.6 Hz, 2H), 8.73 (s, 1H) ppm; ^{13}C NMR (75 MHz, DMSO-d_6): δ 114.5, 123.6, 128.1, 128.7, 129.5, 130.3, 134.1, 145.1, 154.7, 160.9 ppm. IR (Nujol mull): ν 3475 m (NH), 3294 m (NH), 3181 m (NH), 3096 m (=CH), 2270s (CN), 1625 s (C=N) cm^{-1}. Anal. Calcd for $C_{12}H_8N_6$ (236.23): C, 61.01; H, 3.41; N, 35.58; found: C, 60.68; H, 3.22; N, 33.30.

*4.2.1.6. 2-Amino-9-(p-tolyl)-9H-purine-6-carbonitrile (**2f**).* Compound **1f** (0.23 g; 0.92 mmol), acetonitrile and trifluoroacetic acid. Compound **2f** was isolated, after 4 h, as a light yellow solid (0.20 g; 0.80 mmol; 87%). Mp 263–265 °C. ^{1}H NMR (400 MHz, DMSO-d_6): δ 2.36 (s, 3H), 7.12 (s, 2H), 7.37 (d, J = 7.6 Hz, 2H), 7.65 (d, J = 8.4 Hz, 2H), 8.63 (s, 1H) ppm; ^{13}C NMR (100 MHz, DMSO-d_6): δ 20.6, 114.4, 123.5, 128.6, 129.9, 130.2, 131.6, 137.7, 145.1, 154.7, 160.8 ppm. IR (Nujol mull): ν 3502 m (NH), 3310 m (NH), 3292 m (NH), 3099 m (NH), 2164 w (CN), 1638 s (C=N) cm^{-1}. Anal. Calcd for $C_{13}H_{10}N_6$ (250.26): C, 62.39; H, 4.03; N, 33.58; found: C, 62.01; H, 3.88; N, 33.13.

4.2.2. General procedure for the synthesis of 2,5-diamino-6-cyano-4-((phenylamino)pyrimidinium) chloride derivatives 3. 37% Hydrochloric acid (2.5 equiv.) was added to the 2-amino-9*H*-purine-6-carbonitrile **2** solid (0.18–0.87 mmol) in ethanol (10.0–15.0 mL). The reaction mixture was stirred at 80–100 °C, until the starting material was totally consumed, as evidenced by TLC. After 1 day, the green/yellow suspension was cooled in an ice-water bath for a few minutes. The solid was filtered and washed with ethanol and diethyl ether, leading to compounds **3**.

*4.2.2.1. 2,5-Diamino-6-cyano-4-((4-fluorophenyl)amino)-pyrimidinium chloride (**3a**).* Compound **2a** (0.10 g; 0.40 mmol), 37% hydrochloric acid (0.08 mL; 0.39 mmol) and ethanol, 80 °C. Compound **3a** was isolated as a light green solid after 1 day (0.097 g; 0.34 mmol; 85%). Mp 200 °C. ^{1}H NMR (400 MHz, DMSO-d_6): δ 7.23 (t, J = 8.8 Hz, 2H), 7.87 (dt, J_1 = 9.2 Hz, J_2 = 4.8 Hz, 2H), 10.44 (s, 1H) ppm; ^{13}C NMR (100 MHz, DMSO-d_6): δ 98.2, 113.0, 115.5 (d, J = 22 Hz), 125.1 (d, J = 8.0 Hz), 130.1, 133.8 (d, J = 3.0 Hz), 150.9, 153.5, 159.5 (d, J = 242 Hz) ppm. IR: ν 3392 m (NH), 3150 m (NH), 2229 w (CN), 1660 s (C=N), 1651 s (C=N), 1623 s (C=N) cm^{-1}. $C_{11}H_{10}ClFN_6$ (280.72).

*4.2.2.2. 2,5-Diamino-6-cyano-4-((4-chlorophenyl)amino)-pyrimidinium chloride (**3b**).* Compound **2b** (0.10 g; 0.37 mmol), 37% hydrochloric acid (0.08 mL; 0.39 mmol) and ethanol, 100 °C. Compound **3b** was isolated as a dark green solid after 1 day (0.09 g; 0.30 mmol; 81%). Mp 235 °C. ^{1}H NMR (400 MHz, DMSO-d_6): δ 7.44 (dt, J_1 = 8.8 Hz, J_2 = 2.2 Hz, 2H), 7.92 (dt, J_1 = 8.8 Hz, J_2 = 2.2 Hz, 2H), 10.52 (s, 1H) ppm; ^{13}C NMR (100 MHz, DMSO-d_6): δ 98.7, 113.0, 124.5, 128.6, 129.3, 130.1, 136.5, 150.8, 153.3 ppm. IR: ν 3153 m (NH), 2223 w (CN), 1653 s (C=N), 1617 s (C=N) cm^{-1}. $C_{11}H_{10}Cl_2N_6$ (296.03).

*4.2.2.3. 2,5-Diamino-6-cyano-4-((4-bromophenyl)amino)-pyrimidinium chloride (**3c**).* Compound **2c** (0.28 g; 0.89 mmol), 37% hydrochloric acid (0.23 mL; 2.70 mmol) and ethanol, 80 °C. Compound **3c** was isolated as a light brown solid after 1 day (0.22 g; 0.62 mmol; 70%). Mp 241 °C. ^{1}H NMR (400 MHz, DMSO-d_6): δ 7.56 (dt, J_1 = 6.8 Hz, J_2 = 2.0 Hz, 2H), 7.86 (dt, J_1 = 7.2 Hz, J_2 = 2.4 Hz, 2H), 10.74 (s, 1H) ppm; ^{13}C NMR (100 MHz, DMSO-d_6): δ 98.7, 113.0, 117.5, 124.9, 130.1, 131.5, 136.9, 150.8, 153.3 ppm. IR: ν 3554 m (NH), 3153 m (NH), 2224 w (CN), 1652 s (C=N), 1620 s (C=N) cm^{-1}. $C_{11}H_{10}ClN_6Br$ (341.60).

*4.2.2.4. 2,5-Diamino-6-cyano-4-((3-bromophenyl)amino)-pyrimidinium chloride (**3d**).* Compound **2d** (0.06 g; 0.18 mmol), 37% hydrochloric acid (0.05 mL; 0.23 mmol) and ethanol, 100 °C. Compound **3d** was isolated as a light brown solid after 1 day (0.03 g; 0.09 mmol; 50%). Mp 226 °C. ^{1}H NMR (400 MHz, DMSO-d_6): δ 7.33 (t, J = 2.0 Hz, 1H), 7.37 (dt, J_1 = 8.0 Hz, J_2 = 2.0 Hz, 1H), 7.93 (dt, J_1 = 7.6 Hz, J_2 = 2.0 Hz, 1H), 8.05 (t, J = 2.0 Hz, 1H), 10.27 (s, 1H) ppm; ^{13}C NMR (100 MHz, DMSO-d_6): δ 100.6, 113.2, 121.3, 121.5, 124.9, 127.8, 129.7, 130.6, 139.2, 151.2, 153.3 ppm. IR: ν 3168 m (NH), 2223 w (CN), 1652 s (C=N), 1622 s (C=N) cm^{-1}. $C_{11}H_{10}ClN_6Br$ (341.60).

*4.2.2.5. 2,5-Diamino-6-cyano-4-(phenylamino)pyrimidinium chloride (**3e**).* Compound **2e** (0.14 g; 0.58 mmol), 37% hydrochloric acid (0.08 mL; 0.39 mmol) and ethanol, 80 °C. Compound **3e** was isolated as a light yellow solid after 22 hours (0.10 g; 0.38 mmol; 66%). Mp 214 °C. ^{1}H NMR (400 MHz, DMSO-d_6): δ 7.19 (t, J = 7.2 Hz, 1H), 7.39 (t, J = 8.8 Hz, 2H), 7.82 (d, J = 7.6 Hz, 2H), 10.03 (s, 1H) ppm; ^{13}C NMR (100 MHz, DMSO-d_6): δ 97.7, 112.9, 123.0, 125.6, 128.7, 130.2, 137.3, 150.7, 153.4 ppm. IR: ν 3154 m (NH), 2226 w (CN), 1651 s (C=N), 1627 s (C=N), 1600 s (C=N) cm^{-1}. $C_{11}H_{10}ClN_6$ (262.70).

*4.2.2.6. 2,5-Diamino-6-cyano-4-(p-tolylamino)-pyrimidinium chloride (**3f**).* Compound **2f** (0.13 g; 0.53 mmol), 37% hydrochloric acid (0.11 mL; 0.56 mmol) and ethanol, 80 °C. Compound **3f** was isolated as a light green solid after 1 day (0.10 g; 0.34 mmol; 64%). Mp 220 °C. ^{1}H NMR (400 MHz, DMSO-d_6): δ 2.29 (s, 3H), 7.17 (d, J = 8.0 Hz, 2H), 7.69 (dt, J_1 = 8.4 Hz, J_2 = 2.4 Hz, 2H), 9.65 (s, 1H) ppm; ^{13}C NMR (100 MHz, DMSO-d_6): δ 20.6, 97.4, 112.9, 123.0, 129.1, 130.1, 134.7, 134.9, 150.7, 153.3 ppm. IR: ν 3180 m (NH), 2222 w (CN), 1649 s (C=N), 1622 s (C=N) cm^{-1}. $C_{12}H_{13}ClN_6$ (276.06).

4.2.3. General procedure for the synthesis of 2,5-diamino-6-cyano-4-(phenylamino)pyrimidine derivatives 4. To neutralize compound **3**, triethylamine (2.0 equiv.) and ethanol were added to the solid, leading to compound **4**.

*4.2.3.1. 2,5-Diamino-6-cyano-4-((4-fluorophenyl)amino)-pyrimidine (**4a**).* Compound **3a** (0.097 g; 0.34 mmol), triethylamine (0.10 mL; 0.69 mmol) and ethanol, room temperature. Compound **4a** was isolated as a light green solid after 1 minute (0.08 g; 0.33 mmol; 97%). Mp 219 °C. ^{1}H NMR (400 MHz, DMSO-d_6): δ 5.18 (bs, 1H), 5.85 (bs, 1H), 7.14 (dt, J_1 = 8.8 Hz, J_2 = 2.0 Hz, 2H), 7.81 (dt, J_1 = 9.2 Hz, J_2 = 4.8 Hz, 2H), 8.70 (s, 1H) ppm; ^{13}C NMR (100 MHz, DMSO-d_6): δ 115.1 (d, J = 22 Hz), 116.8, 117.9, 122.5 (d, J = 8.0 Hz), 125.9, 135.8 (d, J = 3.0 Hz), 151.7, 155.5, 157.9 (d, J = 239 Hz) ppm. IR: ν 3491 m (NH), 3390 m (NH), 3353 m (NH), 3290 m (NH), 2229 w (CN), 1636 s (C=N), 1617 s (C=N) cm^{-1}. *m*/*z* calcd for $C_{11}H_9FN_6$ 245.094549, found 245.094868.

*4.2.3.2. 2,5-Diamino-6-cyano-4-((4-chlorophenyl)amino)-pyrimidine (**4b**).* Compound **3b** (0.09 g; 0.30 mmol), triethylamine (0.09 mL; 0.60 mmol) and ethanol, room temperature. Compound **4b** was isolated as a dark green solid after 1 minute (0.07 g; 0.27 mmol; 90%). Mp 250 °C. ^{1}H NMR (400 MHz, DMSO-d_6): δ 5.20 (bs, 1H), 5.90 (bs, 1H), 7.34 (dt, J_1 = 7.2 Hz, J_2 = 3.2 Hz, 2H), 7.85 (dt, J_1 = 7.2 Hz, J_2 = 3.2 Hz, 2H), 8.76 (s, 1H) ppm; ^{13}C NMR (100 MHz, DMSO-d_6): δ 116.8, 118.4, 122.0, 126.0, 126.3, 128.3, 138.5, 151.5, 155.5 ppm. IR: ν 3492 m (NH), 3389 m (NH), 3354 m (NH), 3188 m (NH), 2218 w (CN), 1669 s (C=N), 1604 s (C=N) cm^{-1}. *m*/*z* calcd for $C_{11}H_9ClN_6$ 261.064998, found 261.065117.

*4.2.3.3. 2,5-Diamino-6-cyano-4-((4-bromophenyl)amino)-pyrimidine (**4c**).* Compound **3c** (0.22 g; 0.62 mmol), triethylamine (0.19 mL; 1.24 mmol) and ethanol, room temperature. Compound **4c** was isolated as a light yellow solid after 1 minute (0.18 g; 0.59 mmol; 95%). Mp 256 °C. ^{1}H NMR (400 MHz, DMSO-d_6): δ 5.21 (s, 1H), 5.91 (s, 1H), 7.46 (d, J = 8.8 Hz, 2H), 7.81 (d, J = 8.8 Hz, 2H), 8.78 (s, 1H) ppm; ^{13}C NMR (100 MHz, DMSO-d_6): δ 114.3, 116.8, 118.4, 122.5, 126.1, 131.2, 138.9, 151.5, 155.5 ppm. IR: ν 3496 m (NH), 3391 m (NH), 3351 m (NH), 3189 m (NH), 2218 w (CN), 1668 s (C=N), 1634 s (C=N), 1602 s (C=N) cm^{-1}. *m*/*z* calcd for $C_{11}H_9N_6Br$ 305.014483, found 305.014668.

*4.2.3.4. 2,5-Diamino-6-cyano-4-((3-bromophenyl)amino)-pyrimidine (**4d**).* Compound **3d** (0.03 g; 0.09 mmol), triethylamine (0.03 mL; 0.18 mmol) and ethanol, room temperature. Compound **4d** was isolated as a light brown solid after 1 minute (0.02 g; 0.07 mmol; 78%). Mp 216 °C. ^{1}H NMR (400 MHz, DMSO-d_6): δ 5.18 (bs, 1H), 5.95 (bs, 1H), 7.20 (dt, J_1 = 8.4 Hz, J_2 = 1.2 Hz, 1H), 7.26 (t, J = 8.0 Hz, 1H), 7.88 (dt, J_1 = 8.0 Hz, J_2 = 1.2 Hz, 1H), 7.99 (t, J = 2.0 Hz, 1H), 8.74 (s, 1H) ppm; ^{13}C NMR (100 MHz, DMSO-d_6): δ 116.7, 118.7, 119.2, 121.4, 122.5, 125.3, 126.0, 130.5, 141.1, 151.5, 155.5 ppm. IR: ν 3492 m (NH), 3431 m (NH), 3391 m (NH), 3302 m (NH), 3187 m (NH), 2220 w (CN), 1650 s (C=N) cm^{-1}. *m*/*z* calcd for $C_{11}H_9N_6Br$ 305.014483, found 305.014505.

*4.2.3.5. 2,5-Diamino-6-cyano-4-(phenylamino)pyrimidine (**4e**).* Compound **3e** (0.10 g; 0.38 mmol), triethylamine (0.13 mL; 0.76 mmol) and ethanol, room temperature. Compound **4e** was isolated as a light yellow solid after 1 minute (0.08 g; 0.35 mmol; 92%). Mp 231 °C. ^{1}H NMR (400 MHz, DMSO-d_6): δ 5.20 (bs, 1H), 5.85 (bs, 1H), 7.03 (tt, J_1 = 7.2 Hz, J_2 = 1.2 Hz, 1H), 7.31 (tt, J_1 = 8.4 Hz, J_2 = 2.4 Hz, 2H), 7.80 (dt, J_1 = 8.4 Hz, J_2 = 2.4 Hz, 2H), 8.63 (s, 1H) ppm; ^{13}C NMR (100 MHz, DMSO-d_6): ν 116.9, 118.1, 120.6, 122.8, 122.9, 126.0, 128.6, 139.5, 151.7, 155.6 ppm. IR: δ 3476 m (NH), 3376 m (NH), 3167 m (NH), 2225 w (CN), 1615 s (C=N) cm^{-1}. *m*/*z* calcd for $C_{11}H_9N_6$ 227.103971, found 227.104173.

*4.2.3.6. 2,5-Diamino-6-cyano-4-(p-tolylamino)pyrimidine (**4f**).* Compound **3f** (0.10 g; 0.34 mmol), triethylamine (0.12 mL; 0.68 mmol) and ethanol, room temperature. Compound **4f** was isolated as a light green solid after 1 minute (0.07 g; 0.29 mmol; 85%). Mp 247 °C. ^{1}H NMR (400 MHz, DMSO-d_6): δ 2.30 (s, 3H), 7.19 (d, J = 8.0 Hz, 2H), 7.69 (dt, J_1 = 8.4 Hz, J_2 = 2.4 Hz, 2H), 9.65 (s, 1H) ppm; ^{13}C NMR (100 MHz, DMSO-d_6): δ 20.4, 116.9, 117.8, 120.8, 122.5, 125.9, 129.0, 131.9, 136.8, 151.8, 155.6 ppm. IR: ν 3456 m (NH), 3403 m (NH), 3363 m (NH), 3263 m (NH), 3160 m (NH), 2223 w (CN), 1615 s (C=N), 1603 s (C=N) cm^{-1}. *m*/*z* calcd for $C_{12}H_{11}N_6$ 241.119621, found 241.119687.

4.3. DNA interaction assay

Natural double-stranded salmon sperm DNA was obtained from Invitrogen. Compound and DNA stock solutions were prepared in 10^{-2} M Tris-HCl buffer (pH = 7.2), with 10^{-3} M EDTA. The DNA concentration in a number of bases (or phosphate groups) was determined from the molar absorption coefficient, ε = 6600 M^{-1} cm^{-1} at 260 nm. The emission spectra of several solutions with different [DNA]/[**4d**] ratios, using the same compound concentration (5×10^{-6} M), were recorded. The solutions were left for 24 h to stabilize. The absorbance at an excitation wavelength (λ_{exc} = 350 nm) was lower than 0.1 to avoid inner filter effects. All measurements were performed at room temperature (25.0 ± 0.5 °C). Binding analysis of the experimental data was performed according to the McGhee and von Hippel model[24] to determine the intrinsic binding constant and the binding site size.

4.4. Biological studies

4.4.1. Fluorescence microscopy. The stock solutions of the compounds for biological assessment were prepared by dissolving the compounds in DMSO at a concentration of 50 mM and stored at room temperature protected from light.

The *Saccharomyces cerevisiae* strain used in this work was BY4741 (*MATα leu2Δ0 ura3Δ0 his3-Δ1 met15Δ0*). Yeast cells were taken from a frozen stock at −80 °C, streaked on fresh yeast extract-peptone-dextrose plates (YPDA; 1% *w*/*v* yeast extract, Acros Organics, 2% *w*/*v* peptone, Biolife, 2% *w*/*v* D-glucose, and 2% *w*/*v* agar, LabChem), and incubated at 30 °C for 2–3 days before storing at 4 °C. Yeast cultures were prepared by inoculating one colony from a YPDA plate into fresh liquid YPD (YPDA without agar) medium followed by overnight incubation at 30 °C with shaking at 200 revolutions per minute (rpm). Growth was monitored by measuring the optical density at 600 nm (OD_{600}).

S. cerevisiae cultures of strain BY4741 in the exponential growth phase were used for micrograph acquisition by diluting an overnight culture to an $OD_{600}$of ~0.1 and growth under the same conditions to an OD_{600} of ~0.4. For live/dead verification, cells were centrifuged at 7200*g* for 3 min at room temperature (RT), washed with phosphate-buffered saline (PBS, pH 7.2), re-suspended in PBS with 10 μM propidium iodide (PI) and 250 μM of 2,4,5-triaminopyrimidines with incubation at RT for 15 min, and protected from light. For microscopy inspection, the cells were washed and resuspended in PBS. To generate dead-cell samples, cells were heat-killed before staining in a water bath at 80 °C for 2 min.

All microscopic observations were carried out using an Olympus BX-51 epifluorescence microscope equipped with a 100× oil immersion objective lens. Micrographs were obtained with an Olympus DP72 digital camera and using CellSens software and processed with ImageJ (NIH) version 1.54b. At least two independent experiments were conducted.

4.4.2. Liquid culture assay. Synthetic defined (SD) medium was prepared with 0.67% *w/v* Sigma-Aldrich yeast nitrogen base with ammonium sulphate, 2% *w/v* D-glucose, supplemented with L-methionine (80 mg L^{-1}), L-histidine (80 mg L^{-1}), uracil (80 mg L^{-1}), and L-leucine (400 mg L^{-1}), to compensate for auxotrophy. Overnight cultures in SD medium were diluted to OD_{600} ~ 0.1 in fresh SD medium. Cells were transferred to the 96-well plates using a multichannel pipette and treated with different 2,4,5-triaminopyrimidines at a concentration of 500 μM. Blanks were prepared using SD medium and with each compound at the tested concentration. Controls were performed by replacing the solution of the compound with the same volume of DMSO (solvent of the compounds). For each condition, three independent replicas were used with 4 technical replicas each. The microcultures were incubated at 30 °C with shaking at 200 rpm and cell density was assessed by monitoring the OD_{600} using a Multiskan SkyHigh microplate reader. The specific growth rates were determined and normalized relatively to the control. Statistical analysis was performed with GraphPad Prism version 8.0.2 for Windows (GraphPad Software, Boston, Massachusetts, USA, **https://www.graphpad.com**) using one-way ANOVA followed by Dunnett's multiple comparison test to compare with the control conditions. Results with a *p*-value less than 0.05 were considered statistically significant.

Conflicts of interest

There are no conflicts to declare.

Acknowledgements

This work was supported by the Foundation for Science and Technology (FCT-Portugal) under the scope of the strategic funding of CQ-UM (UIDB/00686/2020), CF-UM-UP (UIDB/04650/2020), CBMA (UIDB/04050/2020), CEB (UIDB/04469//2020), MedInUP (UIDB/04308/2020 and UIDP/04308/2020) and the National NMR Network (RNRMN) (PINFRA/22161/2016). We also acknowledge SearchON2 "Revitalization of HPC infrastructure of UMinho" (NORTE 07-0162-FEDER-000086), co-funded by the North Portugal Regional Operational Programme (ON.2 – O Novo Norte), under the National Strategic Reference Framework (NSRF), through the European Regional Development Fund (ERDF).

References

1 S. Kamiloglu, G. Sari, T. Ozdal and E. Capanoglu, *Food Front.*, 2020, **1**, 332–349.
2 M. Tian, Y. Ma and W. Lin, *Acc. Chem. Res.*, 2019, **52**, 2147–2157.
3 Y. Zhao, C. Zhang, J. Liu, D. Li, X. Tian, A. Wang, S. Li, J. Wu and Y. Tian, *J. Mater. Chem. B*, 2019, **7**, 3633–3638.
4 Y. Lai, T. Zhang, W. Song, Z. Li and W. Lin, *Anal. Chem.*, 2021, **93**, 12487–12493.
5 R. W. Sinkeldam, N. J. Greco and Y. Tor, *Chem. Rev.*, 2010, **110**, 2579–2619.
6 W. Xu, K. M. Chan and E. T. Kool, *Nat. Chem.*, 2017, **9**, 1043–1055.
7 M. Legraverend, *Tetrahedron*, 2008, **64**, 8585–8603.
8 M. Bood, S. Sarangamath, M. S. Wranne, M. Grøtli and L. M. Wilhelmsson, *Beilstein J. Org. Chem.*, 2018, **14**, 114–129.
9 Y. Saito and R. H. E. Hudson, *J. Photochem. Photobiol., C*, 2018, **36**, 48–73.
10 S. S. Bag and I. Saito, *Fluorescent Analogues of Biomolecular Building Blocks: Design and Applications*, 2016, pp. 137–173.
11 K. Seio, T. Kanamori and Y. Masaki, *Tetrahedron Lett.*, 2018, **59**, 1977–1985.
12 J. J. Strouse, M. Jegelnik and J. B. Arterburn, *Acta Chim. Slov.*, 2005, **52**, 187–199.
13 F. Fang, J. Xia, S. Quan, S. Chen and G.-J. Deng, *J. Org. Chem.*, 2023, **88**, 14697–14707.
14 L. Yet, *Privileged Structures in Drug Discovery*, John Wiley & Sons, Ltd, 2018, pp. 237–283.
15 J. Yang, Q. Dang, J. Liu, Z. Wei, J. Wu and X. Bai, *J. Comb. Chem.*, 2005, **7**, 474–482.
16 R. K. Robins, K. J. Dille, C. H. Willits and B. E. Christensen, *J. Am. Chem. Soc.*, 1953, **75**, 263–266.
17 K. Leškovskis, J. M. Zaķis, I. Novosjolova and M. Turks, *Eur. J. Org. Chem.*, 2021, **2021**, 5027–5052.
18 M. Brændvang, C. Charnock and L.-L. Gundersen, *Bioorg. Med. Chem. Lett.*, 2009, **19**, 3297–3299.
19 H.-J. Yang, C.-L. Hsu, J.-Y. Yang and W. Y. Yang, *PLoS One*, 2012, **7**, 1–8.
20 A. Orth, R. N. Ghosh, E. R. Wilson, T. Doughney, H. Brown, P. Reineck, J. G. Thompson and B. C. Gibson, *Biomed. Opt. Express*, 2018, **9**, 2943–2954.
21 C. Yang, V. Hou, L. Y. Nelson and E. J. Seibel, *J. Biomed. Opt.*, 2013, **18**, 86012.

22 R. Hulspas, M. R. G. O'Gorman, B. L. Wood, J. W. Gratama and D. R. Sutherland, *Cytometry, Part B*, 2009, **76**, 355–364.
23 J. M. Gonçalves, J. N. D. Gonçalves, A. S. Pêra, N. R. Senhorães, A. R. O. Rodrigues, R. Oliveira, P. J. G. Coutinho, E. M. S. Castanheira and A. M. Dias, *Eur. J. Org. Chem.*, 2023, **26**, e202300176.
24 J. Yin, L. Huang, L. Wu, J. Li, T. D. James and W. Lin, *Chem. Soc. Rev.*, 2021, **50**, 12098–12150.
25 B. Y. Michel, D. Dziuba, R. Benhida, A. P. Demchenko and A. Burger, *Front. Chem.*, 2020, **8**, 112.
26 M. Rosenberg, N. F. Azevedo and A. Ivask, *Sci. Rep.*, 2019, **9**, 6483.
27 C. Kirchhoff and H. Cypionka, *J. Microbiol. Methods*, 2017, **142**, 79–82.
28 J. D. McGhee and P. H. von Hippel, *J. Mol. Biol.*, 1974, **86**, 469–489.
29 A. S. Abreu, E. M. S. Castanheira, P. J. G. Coutinho, M.-J. R. P. Queiroz, P. M. T. Ferreira, L. A. Vale-Silva and E. Pinto, *J. Photochem. Photobiol., A*, 2012, **240**, 14–25.
30 B. Valeur, *Molecular Fluorescence: Principles and Applications*, Wiley–VCH Verlag GmbH, Weinheim, 2001.
31 S. S. Lehrer, *Biochemistry*, 1971, **10**, 3254–3263.
32 G. M. Morris, D. S. Goodsell, R. S. Halliday, R. Huey, W. E. Hart, R. K. Belew and A. J. Olson, *J. Comput. Chem.*, 1998, **19**, 1639–1662.
33 C. G. Ricci and P. A. Netz, *J. Chem. Inf. Model.*, 2009, **49**, 1925–1935.
34 A. R. O. Rodrigues, M. S. D. Carvalho, J. A. V. Cardoso, R. C. Calhelha, M.-J. R. P. Queiroz, P. J. G. Coutinho and E. M. S. Castanheira, *J. Photochem. Photobiol., A*, 2014, **294**, 20–30.
35 V. R. Jadhav, D. A. Barawkar and K. N. Ganesh, *J. Phys. Chem. B*, 1999, **103**, 7383–7385.
36 T. Kimura, K. Kawai and T. Majima, *Org. Lett.*, 2005, **7**, 5829–5832.
37 M. J. Frisch, G. W. Trucks, H. B. Schlegel, G. E. Scuseria, M. A. Robb, J. R. Cheeseman, G. Scalmani, V. Barone, G. A. Petersson, H. Nakatsuji, X. Li, M. Caricato, A. Marenich, J. Bloino, B. G. Janesko, R. Gom-perts, B. Mennucci, H. P. Hratchian, J. V. Ortiz, A. F. Izmaylov, J. L. Sonnenberg, D. Williams-Young, F. Ding, F. Lip-parini, F. Egidi, J. Goings, B. Peng, A. Petrone, T. Henderson, D. Ranasinghe, V. G. Zakrzewski, J. Gao, N. Rega, G. Zheng, W. Liang, M. Hada, M. Ehara, K. Toyota, R. Fukuda, J. Hasegawa, M. Ishida, T. Nakajima, Y. Honda, O. Kitao, H. Nakai, T. Vreven, K. Throssell, J. A. Montgomery Jr., J. E. Peralta, F. Ogliaro, M. Bearpark, J. J. Heyd, E. Brothers, K. N. Kudin, V. N. Staroverov, T. Keith, R. Kobayashi, J. Normand, K. Raghavachari, A. Rendell, J. C. Burant, S. S. Iyengar, J. Tomasi, M. Cossi, J. M. Millam, M. Klene, C. Adamo, R. Cammi, J. W. Ochterski, R. L. Martin, K. Moroku-ma, O. Farkas, J. B. Foresman and D. J. Fox, *Gaussian 09, Revision C.01*, Gaussian, Inc., Wallingford CT, 2016.
38 Fabrizio Santoro and Javier Cerezo, FCclasses3, A code for vibronic calculations.v3-1.0-2-g78ec1d1,2022, **https://www.iccom.cnr.it/en/fcclasses**.
39 F. J. A. Ferrer and F. Santoro, *Phys. Chem. Chem. Phys.*, 2012, **14**, 13549–13563.
40 S. Fery-Forgues and D. Lavabre, *J. Chem. Educ.*, 1999, **76**, 1260–1264.
41 S. R. Meech and D. Phillips, *J. Photochem.*, 1983, **23**, 193–217.